ACS Partner Journal

Journal of the American Society for Mass Spectrometry

pubs.acs.org/jasms

Research Article

Carbene Cross-Linking in Gas-Phase Peptide Ion Scaffolds

Hongyi Zhu, Václav Zima, Emily R. Ding, and František Tureček*

Cite This: *J. Am. Soc. Mass Spectrom.* 2023, 34, 763−774

Read Online

ACCESS | Metrics & More | Article Recommendations | Supporting Information

ABSTRACT: Scaffolds consisting of a peptide, a phthalate linker, and a 4,4-azipentyl group were synthesized and used to study intramolecular peptide−carbene cross-linking in gas-phase cations. Carbene intermediates were generated by UV-laser photodissociation at 355 nm of the diazirine ring in mass-selected ions, and the cross-linked products were detected and quantified by collision-induced dissociation tandem mass spectrometry (CID-MS^n, n = 3−5). Peptide scaffolds containing Ala and Leu residues with a C-terminal Gly gave 21−26% yields of cross-linked products, while the presence of the Pro and His residues decreased the yields. Experiments using hydrogen−deuterium−hydrogen exchange, carboxyl group blocking, and analysis of CID-MS^n spectra of reference synthetic products revealed that a significant fraction of cross-links involved the Gly amide and carboxyl groups. Interpretation of the cross-linking results was aided by Born−Oppenheimer molecular dynamics (BOMD) and density functional theory calculations that allowed us to establish the protonation sites and conformations of the precursor ions. Analysis of long (100 ps) BOMD trajectories was used to count close contacts between the incipient carbene and peptide atoms, and the counting statistics was correlated with the results of gas-phase cross-linking.

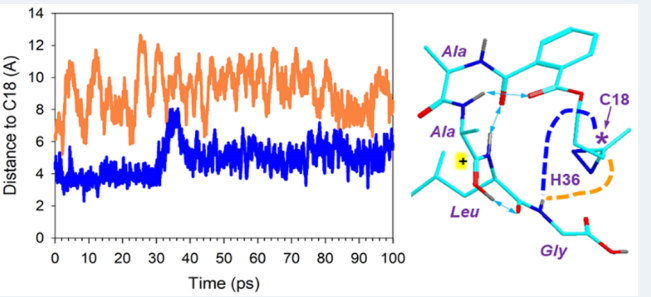

INTRODUCTION

Stable carbene sources, such as diazirines[1−3] and diazoalkanes,[4] have been used extensively in photoaffinity labeling and footprinting studies of various biomolecules.[5−8] The reactive carbene is selectively generated by photodissociation (e.g., at 350−370 nm from diazirines) and reacts rapidly with various bonds in the target molecule. Addition to the double bond[9] and insertion into C−H bonds[10,11] have been studied in detail for simple carbenes and hydrocarbon targets using product analysis,[12−14] EPR spectroscopy,[14] laser flash photolysis,[15] kinetic isotope effects,[16] and quantum mechanical tunneling.[16] The insertion reactions have been found to have very low activation energies.[11−13] In parallel, carbene insertion reactions have been used to achieve covalent cross-linking in noncovalent complexes that almost always involved polar compounds, such as peptides, proteins, and other biomolecules[6,17] where low activation energies were presumed to facilitate covalent bond formation.

This research has received a significant impetus by the development of diazirine-tagged amino acid residues, such as photoleucine and photomethionine, that are recognized by the corresponding leucine and methionine tRNA and can be site-selectively incorporated into proteins.[18] The portfolio of commercially available diazirine-tagged amino acid residues[19] has been expanded to include photoproline[19] and photolysine.[20] We have been developing methods for gas-phase cross-linking in noncovalent complexes of peptides,[21−25] dinucleotides,[26] and small molecules,[27] including specific introduction of the diazirine ring into lysine, cysteine, and at the peptide *N*-terminus.[28] The common feature of all these peptide-related phototags is that the diazirine ring is in an aliphatic chain where it is flanked by CH_2 and CH_3 groups. This makes it possible for the transient singlet carbene to undergo a fast competitive 1,2-hydrogen shift proceeding on a high picosecond to low nanosecond time scale and converting the carbene into an unreactive alkene (Scheme 1).[29−33]

We have taken advantage of this side reaction to use it as an internal clock in our molecular dynamics trajectories of noncovalent complexes that we run on a 100 ps time scale to identify and enumerate close contacts between the incipient carbene atom and the X−H bonds that can potentially undergo insertion. This has allowed us to correlate the computationally determined complex structures and their propensity for amino acid cross-linking with experimental results obtained by photodissociation and product sequence analysis by CID-MS^3.[21−25] The carbene−alkene isomerization is a highly exergonic reaction[34] of $\Delta H_{rxn} \approx -200$ kJ mol^{-1} which often drives dissociation of the rearranged complex.[21−27]

Received: January 25, 2023
Revised: February 26, 2023
Accepted: February 28, 2023
Published: March 7, 2023

https://doi.org/10.1021/jasms.3c00023
J. Am. Soc. Mass Spectrom. 2023, 34, 763−774

Scheme 1. Diazirine Photolysis Products

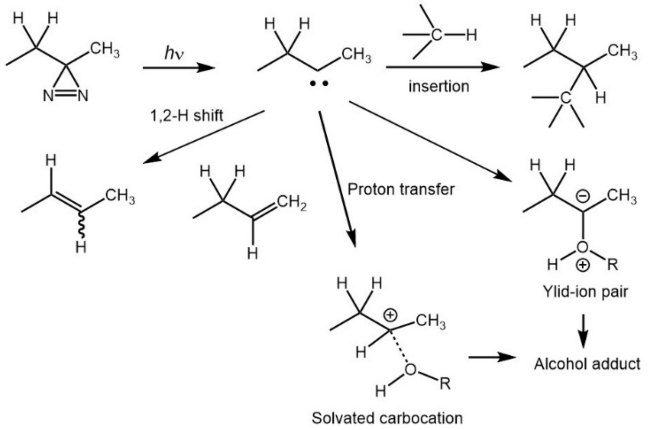

Scheme 2. Scaffolds for Carbene−Peptide Crosslinking Where Peptide Stands for LAAG, ALAG, AALG, AAPG, and AAHG Sequences, Indicating Crosslinks and Alkene Isomerization Products[a]

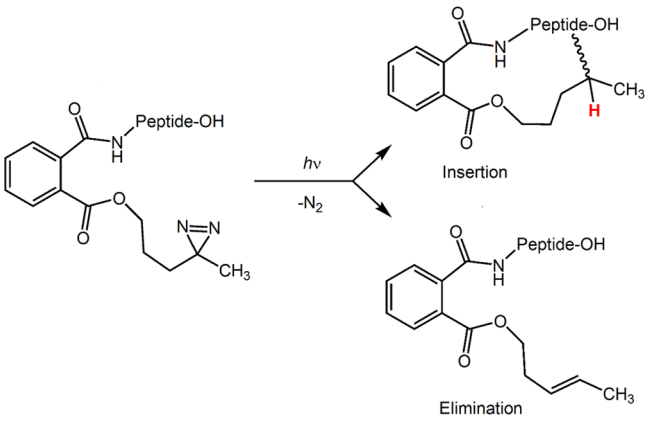

[a]The alternative formation of 4-pentenyl conjugates is not shown.

Whereas carbene reactions with hydrocarbons have been studied in quite a detail, the effect of polar groups on the interaction with carbenes has received less attention that has been focused on small solvent molecules, such as water and alcohols. In a protic solvent, the very high carbene basicity[35,36] favors the formation of a contact pair between the solvent molecule and a carbocation formed by protonation of the transient carbene.[3−42] The contact pair has a short half-life and can collapse to form a C−O bond in the form of an alcohol or ether (Scheme 1).[41] An alternative pathway involves an ylid−ion pair that rearranges to an alcohol by proton migration. Experimental studies of peptide cross-linking in solution have chiefly been of a heuristic nature. A survey of cross-linking yields of a mixture of tryptic peptides with 3,3-azibutan-1-ol, 3,3-azibutan-1-amine, and 4,4-azipentanoic acid gave widely different results depending on the carbene source, amino acid residues in the peptide, and reaction conditions.[43] A solution cross-linking study has reported products that have been presumed to result from carbene coupling to aspartic and glutamic acid forming esters.[44] It has been suggested[44] that the coupling with carboxyl groups results from photochemical isomerization of diazirines to diazoalkanes.[45−47] However, no diazirine isomerization has been detected in gas-phase photoleucine peptide ions by UV−vis and infrared multiphoton dissociation spectroscopies.[48] Interestingly, an intramolecular cyclization between a carbene and a carboxyl group has not been observed in solution.[30]

The previous studies of peptide cross-linking have achieved limited resolution in determining the insertion sites. That was mainly due to incomplete sequencing of the cross-links that narrowed the insertion site to, ideally, one or, more often, a few amino acid residues of the target molecule without specifying the atoms of the X−H bond that were involved in the insertion reaction. We now report a study of carbene cross-linking in model molecular systems that offers the possibility of achieving high spatial resolution regarding the insertion site. Our model consists of a phthalate scaffold that combines the diazirine carbene precursor with the target peptide moiety in one molecule (Scheme 2). This removes issues with complex formation that have been apparent in previous studies of cross-linking in noncovalent complexes.[25,26] The scaffold is readily constructed by stepwise coupling of phthalic anhydride with 4,4-azipentan-1-ol[49] followed by coupling to the peptide chain which is built up on a solid support resin. The synthetic procedures and product characterization are described in the Supporting Information (Schemes S1−S5). Both the size and composition of the peptide moiety are broadly variable. Here, we used peptide sequences consisting of hydrophobic alanine, leucine, and glycine residues, as well as those containing a basic backbone (proline) and side-chain (histidine) residues. This way, one can modify peptide protonation sites and affect the peptide chain conformation. The experimental studies are complemented by computational structure analysis. Using Born−Oppenheimer molecular dynamics (BOMD) and density functional theory (DFT) calculations, we select the lowest energy protomers and conformers for each peptide ion sequence in the scaffolds and determine the dynamics of through-space contacts of the incipient carbene atom with selected atoms and bonds in the peptide moiety in the course of 100 ps trajectories. The combined experimental and computational results bear on achieving a more detailed understanding of carbene based cross-linking to polar biomolecular targets.

EXPERIMENTAL SECTION

Materials and Methods. Standard chemicals were purchased from Sigma-Aldrich (St. Louis, MO) and used as received. Procedures to synthesize peptide scaffolds containing the 4,4-azipentyl, 3-pentene, and 4-pentene side chains are described in detail in the Supporting Information (Schemes S1 and S2). In the first step, the aliphatic C_5-side chain was linked to the aromatic ring as an ester via a reaction with phthalic anhydride. The intermediate ester was then coupled to the *N*-terminus of the peptide chain that was built on a solid support using a standard Fmoc coupling technology.[50] Product purification and characterization by tandem mass spectrometry and NMR spectroscopy is described in the Supporting Information. Benzo[*c*]-6(*S*),9(*S*),18(*R*,*S*)-trimethyl-12(*S*)-2-methylpropyl-1,17-dioxa-5,8,11,14-tetraazacyclohenicosan-2,4,7,10,13,16-hexaone (cyc-s-AALG) was synthesized by a multistep procedure, as described in the Supporting Information (Scheme S4). Mass spectra were measured on a Bruker Daltonik, GmbH (Bremen, Germany), amaZon ion trap mass spectrometer that was equipped with an EKSPLA NL301G Nd:YAG laser (Altos Photonics, Bozeman, MT, USA) working at 20 Hz frequency and 3−6 ns pulse width.

https://doi.org/10.1021/jasms.3c00023
J. Am. Soc. Mass Spectrom. 2023, 34, 763−774

Ions were produced by electrospray ionization, selected by mass in the ion trap, and irradiated by multiple laser pulses at 355 nm. Multistage tandem mass spectra were obtained by collision-induced dissociation (CID) of mass selected fragment ions. The excitation amplitude was chosen to achieve a high conversion of precursor ions.

Calculations. Born−Oppenheimer molecular dynamics (BOMD) calculations were run as 20 ps trajectories with 1 fs steps at 350−600 K using PM6-D3H4 calculations, as described previously.[51] The BOMD calculations were run under the high-level Cuby4 platform.[52] The initial ion structures were constructed with different protonation sites that were at the peptide amide carbonyls for the nonbasic peptides (Ala, Leu, Gly, Pro) and the imidazole side chain for His. In addition to thermal conformational motion, BOMD allows bond changes to proceed along the trajectory, namely, proton migration between different sites in the ion. The 20,000 structures generated by BOMD were sampled at regular intervals, and 200 selected snapshots were fully optimized by PM6-D3H4. This augmented semiempirical procedure has been shown to capture hydrogen bonding and dispersion interactions,[53] and we have used it previously for structure analysis of several gas-phase peptide ions.[21−27] The PM6-D3H4-optimized structures were sorted out by type and energy, and 15−20 low-energy ions were reoptimized with density functional theory (DFT) calculations, using B3LYP[54] and the 6-31+G(d,p) basis set and including harmonic frequency analysis. Several low-energy B3LYP structures were reoptimized with M06-2X[55] and the 6-31+G(d,p) basis set. These were used for single-point energy calculations that were carried out with M06-2X/6-311++G(2d,p) to provide relative energies that were combined with B3LYP zero-point vibrational energies, enthalpies, and entropies to obtain relative Gibbs energies for ion conformers and protomers. Ion solvation energies were estimated from self-consistent reaction field polarizable continuum model calculations (PCM)[56] in water dielectric with full gradient optimization by M06-2X/6-31+G(d,p) and single-point M06-2X/6-311++G(2d,p) energies. These standard DFT calculations were carried out with the Gaussian 16 suite of programs (Revision B.01) that was licensed from Gaussian, Inc. (Wallingford, CT). The lowest energy ion structures from the M06-2X calculations were then used as initial geometries for 100 ps BOMD trajectory runs using Cuby4, where each created 100,000 snapshots for atom−atom contact analysis.

RESULTS AND DISCUSSION

Photodissociation and Cross-Linking Yields. Scaffold ions s-LAAG, s-ALAG, and s-AALG (m/z 575), s-AAPG (m/z 559), and s-AAHG (m/z 599) were produced by electrospray protonation from aqueous-methanol solutions and selected by mass in the ion trap. Photodissociation at 355 nm resulted in elimination of N_2 from the diazirine ring and formation of product ions (Figure 1a−c, Figure 2a,b). Although photolysis at 355 nm is highly specific for breaking the diazirine ring in the scaffolds, the pertinent $\pi_{xy} \rightarrow \pi_z$ electronic transition is dipole disallowed,[1] making the photolysis inefficient. We used multiple (>10) laser pulses to achieve conversions that produced photodissociation ion counts allowing further ions analysis by multistage collision-induced dissociations tandem mass spectrometry (CID-MS^n). Loss of N_2 was accompanied by consecutive dissociations that were driven by the substantial exergonicity of carbene insertion[27] or isomerization.[34] We

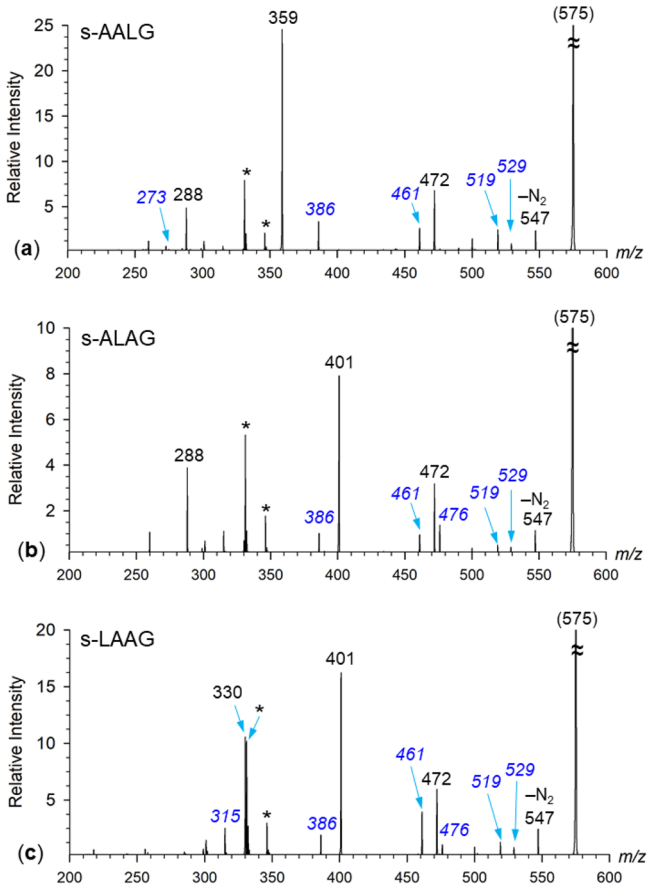

Figure 1. UVPD-MS^2 spectra (355 nm) of m/z 575 ions from protonated (a) s-AALG, (b) s-ALAG, and (c) s-LAAG. Fragment ions originating from cross-linked photoproducts are annotated by blue italic numerals. Ions from laser desorption-ionization of surface material are denoted by asterisks.

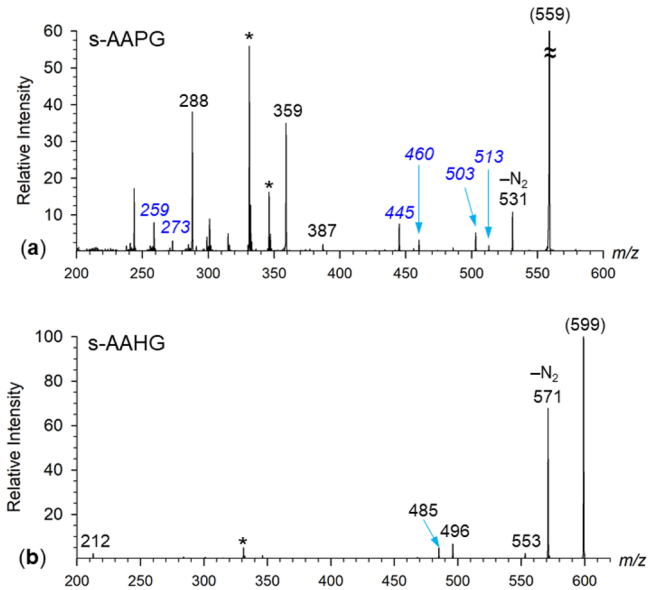

Figure 2. UVPD-MS^2 spectra (355 nm) of protonated (a) s-AAPG at m/z 559 and (b) s-AAHG at m/z 599. Fragment ions originating from cross-linked photoproducts are annotated by blue italic numerals. Ions from laser desorption−ionization of surface material are denoted by asterisks.

https://doi.org/10.1021/jasms.3c00023
J. Am. Soc. Mass Spectrom. 2023, 34, 763−774

found tetrapeptide scaffolds to be the smallest ones to provide fractions of stable $(MH - N_2)^+$ ions for further CID-MS^n studies. The fragment ions formed by photodissociation were identified with the help of CID-MS^n spectra of the surviving $(MH - N_2)^+$ ions and synthetic 3-pentene and 4-pentene derivatives representing the byproducts of carbene isomerization to alkenes.

Reference CID-MS^n spectra of the alkene derivatives are presented in Figure S1a–c (Supporting Information). For s-AALG, s-ALAG, and s-LAAG, CID-MS^n of their pentene esters showed simple peptide backbone cleavages resulting in the sequential loss of the amino acid residues starting with GlyOH and followed by Leu or Ala according to the particular sequence. These fragment ions were used to identify and quantify cross-links and non-cross-link olefin byproducts from diazirine photodissociation.

Photodissociation spectra of s-AALG, s-ALAG, and s-LAAG that were obtained with 14 laser pulses gave conversions ranging between 16 and 35% (Table 1). The overall

Table 1. Photodissociation Conversion and Cross-Link Yields

Conjugate	Laser Pulses (%)	UVPD Conversion[a] (%)	Survivor Fraction[b] (%)	Cross-Link Fraction[c] (%)
s-AALG	14	35	4.7	21
s-ALAG	14	16	4.5	25
s-LAAG	14	29	4.6	26
s-AAPG	36	49	6.4	11
s-AAHG	14	43	83	7.8
s-AALG-OEt	36	65	2.5	13

[a]Fraction of total UVPD produced ions. [b]Fraction of nondissociating $(MH - N_2)^+$ ions relative to the total photoproduct ion intensities. [c]Fraction of photoproducts identified as originating from cross-links.

conversion depended on the laser power and overlap of the ion cloud with the laser beam in the ion trap that varied in measurements taken on different days. Internal normalization of the photoproducts showed nondissociating (survivor) fractions of 4.5–4.7% for s-AALG, s-ALAG, and s-LAAG (Table 1). The orthogonal nature of the cross-link and non-cross-link CID-MS^n spectra allowed us to clearly distinguish these populations. Photodissociation of s-AALG, s-ALAG, and s-LAAG was found to produce 21–26% fractions of cross-linked ions (Table 1). The s-AAPG ion gave a somewhat higher photodissociation yield (49%) and lower yields of both the survivor fraction (6.4%) and cross-link products (11%). The last two figures were even more pronounced for s-AAHG which gave nondissociating photoproducts at 83% but only a 7.8% yield of fragments assigned to cross-links. We note that the cross-link yields from the peptide scaffolds were in the middle range of yields typically obtained from gas-phase noncovalent peptide–peptide complexes[21−25] and orders of magnitude higher than yields of cross-links for equimolar carbene–substrate ratios in solution.[43,44]

CID-MS^n Analysis of Cross-linked Photoproducts. The $(MH - N_2)^+$ ions from diazirine photodissociation were further investigated by CID-MS^3. The $(MH - N_2)^+$ ions at m/z 547 from s-AALG, s-ALAG, and s-LAAG gave very similar fragmentation patterns in which the fragment ions were identified on the basis of accurate mass measurements of analogous $(MH - N_2)^+$ ions that were separately generated by CID-MS^2 of the scaffolds. The conspicuous feature of the CID-MS^3 spectra (Figure 3a–c) was that they showed a very minor

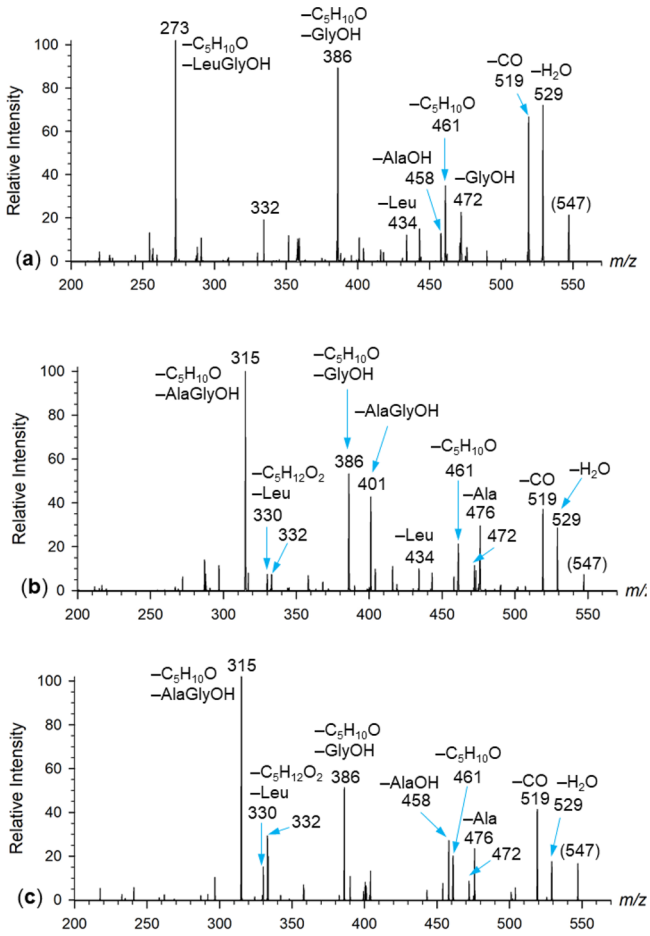

Figure 3. CID-MS^3 spectra of m/z 547 ions from photodissociation of (a) s-AALG, (b) s-ALAG, and (c) s-LAAG. Fragment ions and neutral losses were assigned from accurate mass measurements.

loss of GlyOH (m/z 472), which was the dominant dissociation of non-cross-linked scaffold ions. Instead, the spectra showed losses of water, CO, and $C_5H_{10}O$ from the side chain (m/z 461) and a loss of an out-of-sequence alanine residue at m/z 476 and 458. These features, including sequence scrambling, are typical of cyclic peptides,[57,58] affirming that the ions were internal cross-links in which the peptide and alkyl side chains were connected by a covalent bond. The loss of $C_5H_{10}O$ from the side chain was combined with loss of GlyOH (m/z 386) and dipeptide sequence residues LeuGlyOH (m/z 273) and AlaGlyOH (m/z 315) (Figure 3a–c, respectively). This interpretation was corroborated by the CID-MS^4 spectra of m/z 461 ions that showed the pertinent peptide sequence fragment ions as dominant products (Figure S2a–c, Supporting Information). The facile loss of $C_5H_{10}O$ upon CID indicated that the C–X bond forming the cross-link to the peptide chain was susceptible to proton driven cleavage. This feature is typical of ester C–O and amide C–N bonds but not aliphatic C–C bonds, suggesting that the carbene insertion into the AALG, ALAG, and LAAG sequences involved the peptide amide N–H and/or glycine carboxyl O–H bonds.

The CID-MS^3 spectrum of the survivor $(MH - N_2)^+$ ions from s-AAPG showed fragment ions indicating a cyclic peptide

https://doi.org/10.1021/jasms.3c00023
J. Am. Soc. Mass Spectrom. 2023, 34, 763–774

structure (m/z 531, Figure 4a). These were formed by loss of CO (m/z 503) and Ala (m/z 460) combined with water (m/z

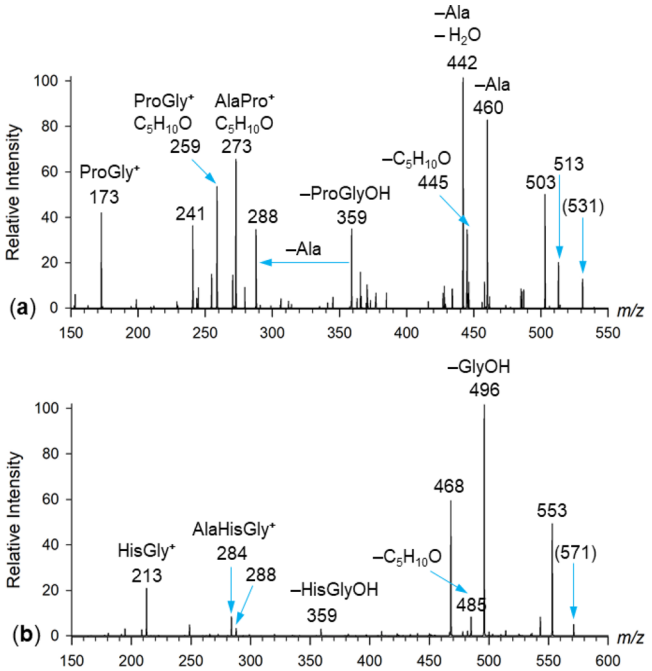

Figure 4. UVPD-MS^3 spectra of ions from photodissociation of (a) s-AAPG (m/z 531) and (b) s-AAHG (m/z 571).

442) and $C_5H_{10}O$ (m/z 445). Interestingly, the loss of the $C_5H_{10}O$ side chain was not accompanied by loss of glycine. The side chain appeared to be conjugated to the proline residue, as evidenced by the $C_5H_{10}O$-ProGly$^+$ (m/z 259) and Ala-$C_5H_{10}O$-Pro$^+$ (m/z 273) ions. At the same time, the spectrum also displayed fragment ions compatible with noncyclized structures, such as the m/z 359 and m/z 288 sequence ions. Note that these ions also appeared prominently in the CID-MS^2 spectrum of the AAPG-alkene byproduct (m/z 531, Figure S3a). The internal cleavage ion from UVPD-CID-MS^3 of s-AAPG (m/z 460, loss of Ala) was further examined by its CID-MS^4 spectrum (Figure S3b) that displayed loss of $C_5H_{10}O$ (m/z 374) combined with loss of glycine (m/z 299). Since an inverse sequence of losses, that is, glycine followed by $C_5H_{10}O$, was not observed (Figure S3b), this seemed to indicate cross-linking via a glycine ester. Along with the other dissociations, the spectra indicated that the $(MH - N_2)^+$ ions from s-AAPG were a mixture of linear and cyclized isomers.

The CID-MS^3 spectrum of the abundant survivor $(MH - N_2)^+$ ions from s-AAHG (m/z 571, Figure 4b) showed features that indicated predominant alkene products. This was inferred from the similarity with the CID-MS^2 spectrum of the authentic AAHG-pentene standard (Figure S4). Thus, the carbene generated in the histidine-containing scaffold chiefly underwent a rearrangement to an alkene or alkenes.

Determination of Cross-Link Sites in s-AALG by H/D Exchange and Reference Spectra of Synthetic Standards. The CID-MS^n analysis of the photodissociation products from s-AALG, s-ALAG, and s-LAAG ions in the gas phase indicated the possibility of the formation of cross-links with cyclized lactone or amide structures. We carried out further experiments to investigate the cross-link's structure for s-AALG. According to the standard mechanism of X–H bond insertion into carbenes (Scheme 1), the hydrogen atom involved is incorporated in a stable covalent C–H bond. This means that protons from polar O–H or N–H bonds that are prone to hydrogen–deuterium exchange in the reactant become nonpolar if involved in carbene insertion and cannot be further affected by prototropic H/D exchange. To probe cross-linking in s-AALG, we converted all five exchangeable amide N–H and carboxyl O–H protons to deuterons under mild nonacidic conditions and subjected the sample to UV photolysis in CD_3OD/D_2O solution (Schemes S3 and S4, Supporting Information). The products were then converted back to the protic cycle and analyzed by tandem mass spectrometry. The electrospray mass spectrum showed partial retention of deuterium in the $(MH - N_2)^+$ ion at m/z 548, whereas the main fraction was back exchanged (m/z 547, Figure 5a, inset). CID-MS^2 of the m/z 548 ion indicated that

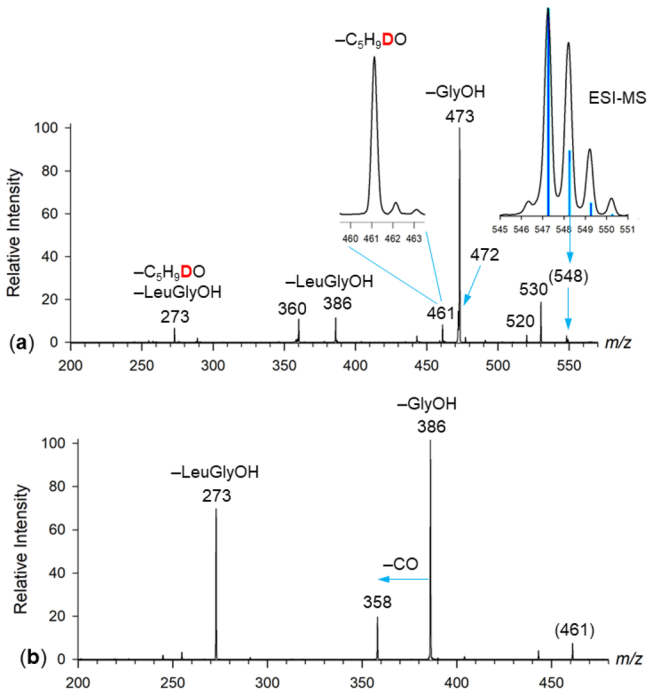

Figure 5. (a) CID-MS^2 of the m/z 548 D_1-containing ion from solution photolysis of 4,4-azipent-1-yl-[D_5]-AALG and back D → H exchange. Insets show the precursor ion cluster at m/z 545–551 with theoretical isotope distribution, and the peak profile of the m/z 461 fragment ion. (b) CID-MS^3 of m/z 461.

the products of solution photolysis chiefly consisted of alkene isomers, as judged by the loss of glycine and Leu-Gly molecules, giving rise to the respective m/z 473 and 386 fragment ions. We note that the m/z 548 ion contained ca. 40% of combined ^{13}C and ^{15}N isotopologues of the m/z 547 ion that were unresolved from the m/z 548 D_1 species and contributed to the formation of the m/z 473 and 386 fragment ions. However, the m/z 461 fragment ion in the CID-MS^2 spectrum signified a loss of C_5H_9DO that was further corroborated by the combined loss of C_5H_9DO and LeuGly (m/z 273, Figure 5a). The CID-MS^3 spectrum of the m/z 461 ion (Figure 5b) confirmed there was no deuterium present after the loss of C_5H_9DO. This established that an exchangeable proton was incorporated into the transient carbene upon photolysis.

https://doi.org/10.1021/jasms.3c00023
J. Am. Soc. Mass Spectrom. 2023, 34, 763–774

Scheme 3. Carbene Interactions with OH and NH Bonds in s-AALG Peptide Scaffolds

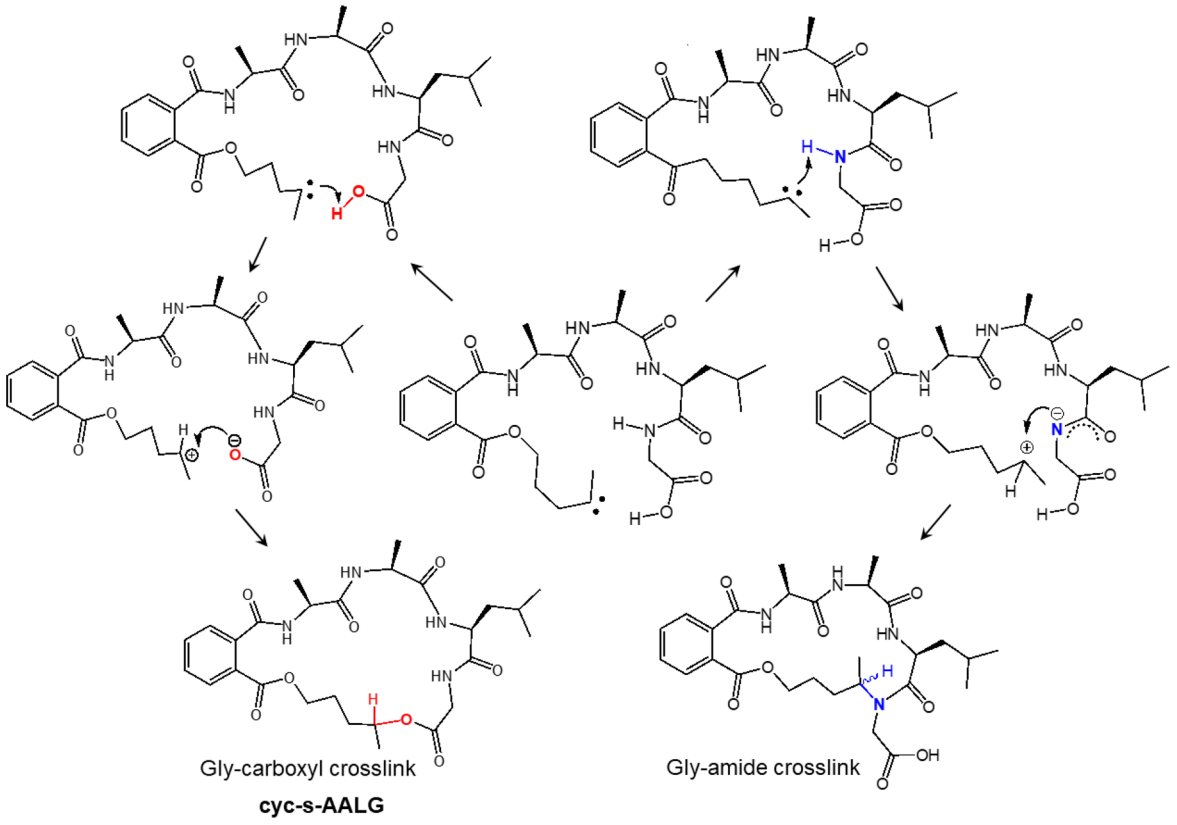

To further specify the peptide functional group engaged in cross-linking, we studied gas-phase photodissociation of s-AALG-OC_2H_5 in which the C-terminal carboxyl group was blocked as an ethyl ester. Table 1 data show that photodissociation of s-AALG-OC_2H_5 proceeded with a smaller survivor $(MH - N_2)^+$ and cross-link fractions when compared to those from s-AALG. This ca. 40% decrease was interpreted as being due to the formation of alkene products caused by the carboxyl blockage. This was corroborated by both the UVPD-MS^2 of s-AALG-OC_2H_5 at m/z 603 and CID-MS^3 of the $(MH - N_2)^+$ ion at m/z 575, as shown in Figure S5a,b, respectively.

UVPD of s-AALG-OC_2H_5 showed substantial dissociation of the peptide chain which was typical of the alkene products of N_2 elimination. CID-MS^3 of the $(MH - N_2)^+$ ion showed less abundant m/z 472 (loss of $GlyOC_2H_5$) and m/z 359 (loss of $LeuGlyOC_2H_5$) sequence ions that would be indicative of an alkene ion where this dissociation predominated (Figure S5c). Prominent dissociations in the ester group by loss of ethylene and ethanol, m/z 547 and 529, respectively, were accompanied by nonsequence loss of Ala (m/z 504) and Leu (m/z 462) that indicated the presence of cross-links. Remarkably, loss of $C_5H_{10}O$ from the side chain (m/z 386) was observed only following the loss of $GlyOC_2H_5$, so this fragmentation could not be used as a cross-link signature.

The results from H/D exchange and carboxyl blocking experiments can be summarized as follows. Polar amide and carboxyl groups significantly participate in cross-linking to the transient carbene produced in the scaffold side chain. A fraction, estimated at about 40% of polar cross-links, is due to participation by the carboxyl OH group forming a lactone product. The other fraction involves one of the amide N−H bonds, specifically that between Leu and Gly in s-AALG, forming a cyclic amide product. Scheme 3 depicts the possible pathways from the carbene intermediate to the carboxyl and amide cross-links. The cross-link creates a chiral center at the former carbene atom which most likely gives rise to racemic products. The efficiency of these pathways, which totals up to 21% according to Table 1 data, depends on the kinetics of the first step, which presumably consists of a proton transfer to the electron-rich carbene.[38,39] This step depends on the populations of ion conformations in thermal ions that determine the probability of the proton to appear at a distance to the carbene atom allowing C−H bond formation in the transient carbocation. Conformations in which the proton is remote from the carbene undergo competitive isomerization within the side chain by 1,2-hydrogen migration from the adjacent CH_2 or CH_3 group to form alkene isomers.

To further elucidate the carboxyl participation in carbene quenching, we synthesized an authentic lactone corresponding to the Gly-carboxyl cross-linked product, denoted cyc-s-AALG in Scheme 3. The CID-MS^2 spectrum of protonated cyc-s-AALG (m/z 547) showed fragment ions by loss of water, GlyOH, $C_5H_{10}O$, $(C_5H_{10}O + H_2O)$, $(C_5H_{10}O + GlyOH)$, and LeuGlyOH at m/z 529, 472, 461, 443, 386, and 359, respectively (Figure 6a). These fragment ions, which were characteristic of a cyclic structure, also appeared in the CID-MS^3 spectrum of the s-AALG UVPD product, although with different relative intensities (cf. Figure 3a).

In particular, the UVPD product showed a more prominent loss of CO (m/z 519) and the combined loss of $C_5H_{10}O$ and LeuGlyOH (m/z 273). On the basis of the Gly ethyl ester blocking results (Table 1), we estimated the content of the lactone form of cyc-s-AALG at ca. 40%, which allowed us to subtract this contribution from the spectrum of the UVPD

https://doi.org/10.1021/jasms.3c00023
J. Am. Soc. Mass Spectrom. 2023, 34, 763−774

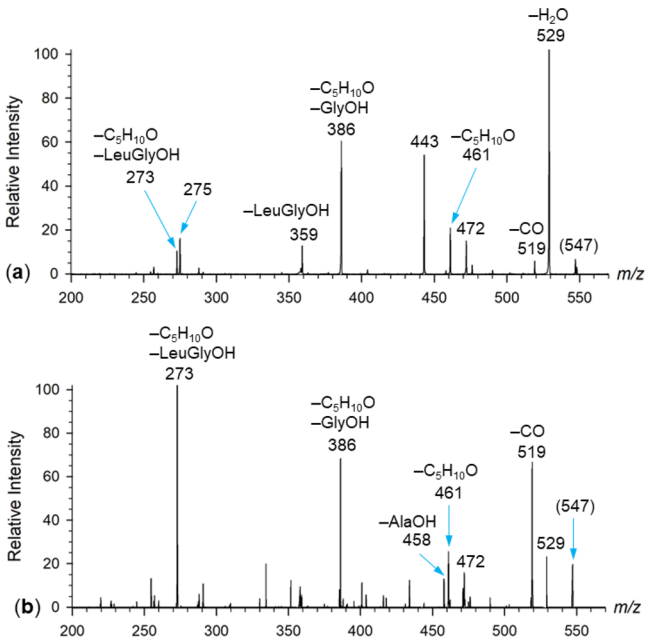

Figure 6. (a) CID-MS^2 of the m/z 547 ion from cyc-s-AALG. (b) Difference spectrum of m/z 547 CID-MS from UVPD of 4,4-azi-pent-1-yl-s-AALG and cyc-s-AALG.

product. The resulting renormalized difference spectrum (Figure 6b) showed the dominant dissociations by combined losses of $C_5H_{10}O$ and the GlyOH and LeuGlyOH fragments. Along with the results of deuterium labeling, this indicated that the cross-linking involved the N−H bond of the Gly amide, as shown in Scheme 3. However, on the basis of the experimental data we cannot exclude cross-linking to the N−H bond of the Leu amide. It should be noted that increasing the amide group basicity by N-alkylation, as in the amide cross-links, has been reported to enhance peptide bond cleavage,[59] which was consistent with the facile backbone dissociations at the cross-linked residues in the Figure 6b spectrum.

The dissociations of the cyc-s-AALG lactone isomer were further investigated with the help of deuterium labeling in the N-D exchanged D_5-derivative (Figure S6, Scheme S5, Supporting Information). The spectrum showed a combined loss of HDO and D_2O, indicating ester elimination and lactone ring opening that involved light hydrogens from the aliphatic side chain. Consistent with this, the losses of GlyOH and LeuGlyOH were comprised of D_1−D_3-containing molecules, indicating the involvement of light hydrogens. In contrast, the loss of $C_5H_{10}O$ did not involve any H/D exchange, which suggested that this neutral molecule was eliminated as a cyclic ether. Note that an elimination of $C_5H_{10}O$ as a pentenol would have necessarily involved a deuteron transfer onto the neutral molecule.

Structures of s-AALG Peptide Ions. To interpret the results of scaffold photodissociation and carbene cross-linking, we carried out extensive calculations of ion structures and dynamics. The main aims of these calculations were to determine the most energetically favorable protonation sites and ion conformations of the diazirine-containing scaffolds and to analyze dynamic contacts between the incipient carbene atom and peptide bonds in thermal ions. BOMD calculations of s-AALG ions were carried out with initial structures protonated at the phthalate, Ala1, Ala2, and Leu amides. Several low Gibbs energy structures are shown in Figure 7. Structures initially protonated at Ala1, Ala2, and Leu collapsed upon BOMD to a single protomer that carried the proton at the Ala2 amide. In the lowest energy structures (**A1**−**A4**) the Ala2 proton was shared by a very short (1.39−1.47 Å) hydrogen bond with the Leu amide, indicating a very facile proton migration between these two amide groups. This hydrogen bond locked the conformation of the Ala2-Leu segment of the peptide chain which moved as a unit in thermal motion of the ions. Ions **A1**−**A4** chiefly differed in the conformation of the leucine and diazirine-carrying side chains.

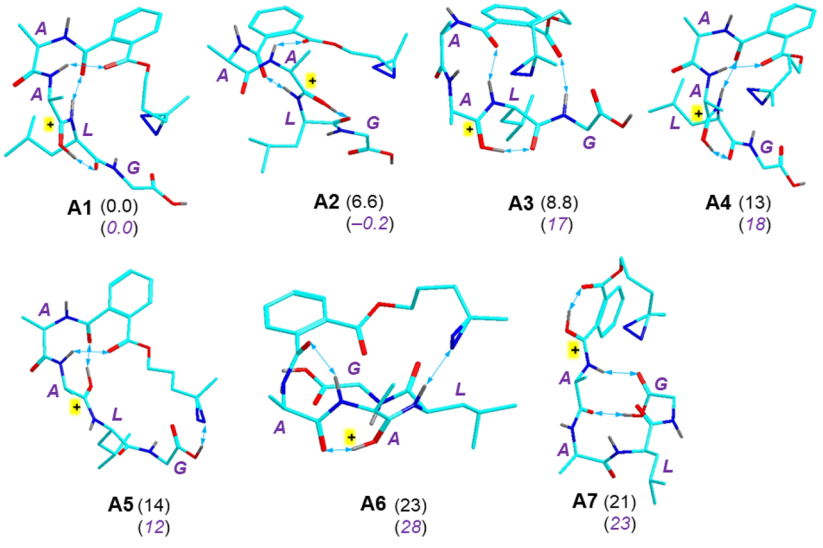

Figure 7. M06-2X/6-31+G(d,p)-optimized structures of low-energy s-AALG ions. Atom color coding is as follows: cyan = C, blue = N, red = O, gray = H. Only exchangeable hydrogens are shown to avoid clutter. Hydrogen bonds are indicated by double-headed blue arrows. The protonated amide groups are labeled with plus signs. Relative Gibbs energies in kJ mol^{-1} are from M06-2X/6-311++G(2d,p) single-point energy calculations including B3LYP zero-point energies, enthalpies, and entropies and referring to 310 K. Relative Gibbs energies of water-solvated ions are shown as purple italics.

https://doi.org/10.1021/jasms.3c00023
J. Am. Soc. Mass Spectrom. 2023, 34, 763−774

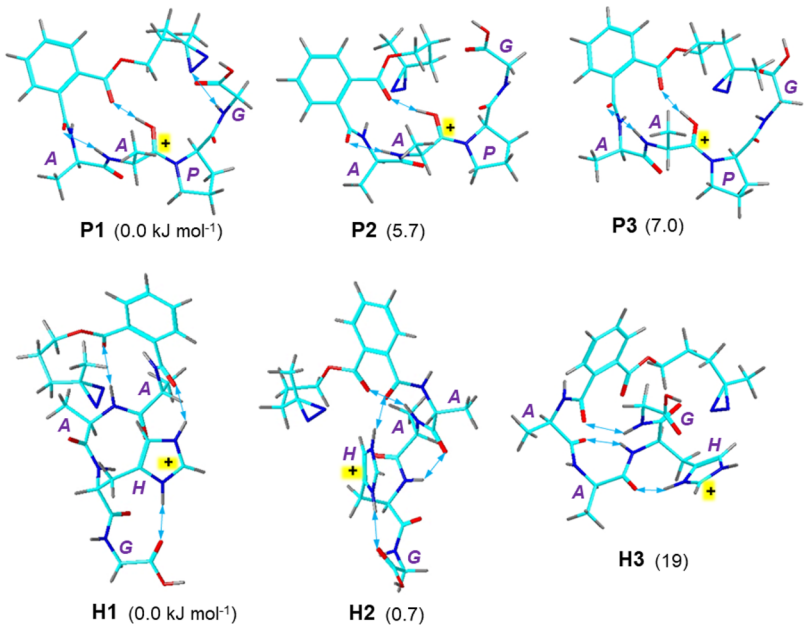

Figure 8. M06-2X/6-31+G(d,p)-optimized structures of low-energy s-AAPG and s-AAHG ions. Description as in Figure 7.

Table 2. Interatomic Distances in Peptide Scaffolds of the Incipient Carbene Atom C18 to Selected Atoms

		Distance (Å)[a,b]						
Scaffold	Ion	COOH	COO**H**	Gly-NH	Gly-N**H**	Leu-NH	Leu-N**H**	Ala2-O**H**
s-AALG	**A1**	5.14	5.57	4.26	4.41	4.90	5.89	5.26
	A2	6.86	7.78	5.38	6.27	5.46	6.03	4.15
	A3	5.49	5.38	4.63	4.38	4.18	3.73	5.49
	A4	12.0	12.7	9.72	10.2	7.53	7.36	7.85
	A5	4.1	3.22	6.34	6.57	7.30	7.12	8.50
	A6	8.94	9.50	6.61	7.07	4.49	3.51	7.36
s-AAPG	**P1**	5.38	5.59	4.44	3.67			5.10
	P2	7.74	7.54	6.66	6.28			4.06
	P3	3.58	3.88	4.16	4.55			4.39
s-AAHG	**H1**	10.9	11.2	8.07	7.83			
	H2	10.7	10.5	9.12	9.27			
	H3	7.39	7.77	5.83	6.53			

[a]Atoms of interest shown with bold letters. [b]Based on M06-2X/6-31+G(d,p) optimized geometries.

Structures **A5** and **A6** had different conformations in which the Ala2 proton was hydrogen bonded to the phthalate and Ala1 amide carbonyls at 1.49 and 1.38 Å, respectively. The phthalate-protonated ion **A7** was another higher energy protomer. Nevertheless, the Gibbs energy differences among the various protomers and conformers were small enough to allow proton migrations among the amide groups as well as ensuring a conformational mobility of the peptide C-terminus and side chain in thermal ions.

Solvation by water, as estimated from polarizable continuum model calculations, equalized the relative Gibbs energies of **A1** ($\Delta G_{310,\,aq}$ = 0.0 kJ mol^{-1}) and **A2** ($\Delta G_{310,\,aq}$ = −0.2 kJ mol^{-1}) while those of **A3**−**A6** remained at $\Delta G_{310,\,aq}$ > 12 kJ mol^{-1} (Figure 7). This indicated that solvent effects that may play a role in ion charging in electrospray droplets were comparable for all s-AALG ion protomers and conformers and were unlikely to significantly change the populations of gas-phase ions.

Structures of s-AAPG and s-AAHG ions. The presence of the basic residues in s-AAPG and s-AAHG suggested preferential protonation at the Pro tertiary amide and His imidazole ring, respectively, in the gas-phase ions. Indeed, initial s-AAPG ion structures in which the proton was placed at different amide groups converged to Pro-protomers upon BOMD. The lowest Gibbs energy structures (**P1**−**P3**) showed the same peptide pattern of the protonated tertiary amide at Pro, forming a strong hydrogen bond to the phthalate ester carbonyl (Figure 8). These nearly isoenergetic structures differed in the conformation of the diazirine-carrying side chain that affected the distance between the incipient carbene atom (C18) and the peptide atoms. In particular, structure **P3** showed very short distances to C18 of the carboxyl OH and Gly amide NH that were 3.58 and 4.16 Å, respectively (Table 2).

Low-energy s-AAHG ions were all protonated at the His imidazole nitrogens. This allowed the ions to form hydrogen bonds clamping the peptide chain conformations in an extended conformation in the lowest energy structures **H1** and **H2** (Figure 8), whereas the diazirine-carrying side chain was relatively free to move. Structure **H3** of a higher energy had a more tightly folded conformation due to multiple hydrogen bonds between the neutral amide groups.

https://doi.org/10.1021/jasms.3c00023
J. Am. Soc. Mass Spectrom. 2023, 34, 763−774

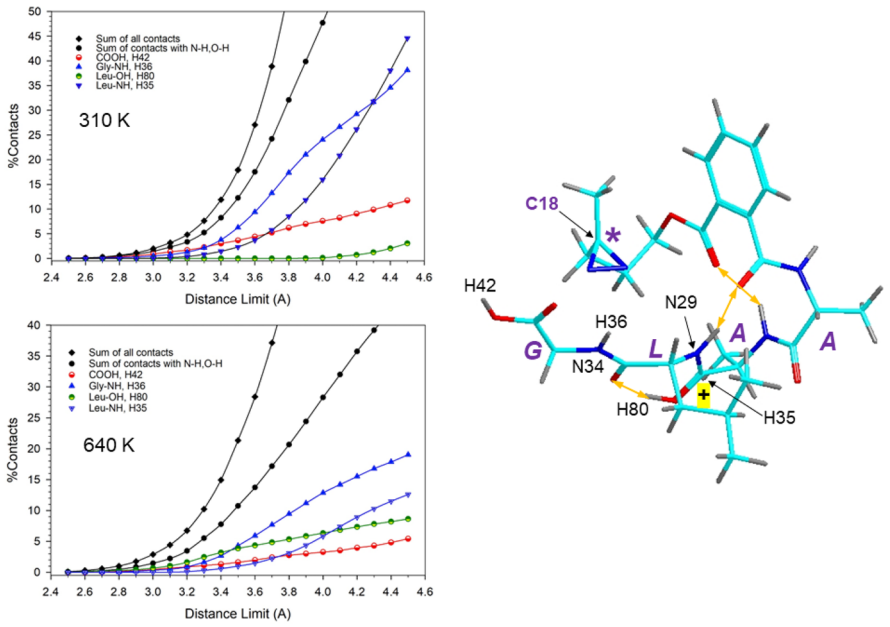

Figure 9. Contact analysis of 100 ps BOMD trajectories of ion **A1** at 310 K (top) and 640 K (bottom). For atom number assignment see the structure on the right; the incipient carbene (C18) is annotated with an asterisk. The limits in Å are cutoffs for counting the number of interatomic distances to C18 in the 100 ps trajectories. The total fractions are overcounted due to simultaneous contacts with multiple atoms.

Atom−Atom Contact Analysis of Thermal Ions in the Course of 100 ps BOMD Trajectories. The fully optimized geometries of the low Gibbs energy peptide scaffold ions represented static local energy minima in which the incipient carbene atoms could be remote from the carboxyl oxygen and amide nitrogen atoms that were engaged in photodissociative cross-linking. For example, the stationary distance between the incipient carbene atom (C18) and the carboxyl hydroxyl O41, Gly-amide N34, and Leu amide N29 in structure **A1** was 5.14, 4.26, and 4.90 Å, respectively. For the list of selected interatomic distances see Table 2. In contrast to the calculated ion geometries at local energy minima that corresponded to static structures at 0 K, the gas-phase ions we studied experimentally were in the buffer gas at the ion trap temperature (310 K). Thus, thermal motion of all atoms and the ensuing conformational changes had to be considered to capture and map temporary variations of interatomic distances between the incipient carbene atom (C18) and selected atoms in the peptide chain. Furthermore, photodissociation resulted in internal excitation of the nascent carbene ion that can be expressed by assigning it an effective temperature. According to our calculations, dissociation of **A1** to N_2 and the carbene intermediate was 59 kJ mol^{-1} endergonic. When combined with the photon energy (337 kJ mol^{-1} at 355 nm) and standard **A1** rovibrational enthalpy (100 kJ mol^{-1} at 310 K), 378 kJ mol^{-1} will be be distributed between the carbene ion and the departing N_2 molecule. Although we did not know the kinetic energy of the departing N_2 molecule to exactly evaluate the internal energy distribution in the products, we could estimate the carbene ion effective temperature at 640 K, as an upper limit corresponding to 378 kJ mol^{-1} rovibrational energy. The hot nascent carbene ion then underwent cooling collisions with the bath gas, limiting the ion internal excitation to within the 310−640 K range.

In the contact analysis, we considered that the diazirine ring limits the closest approach of the peptide atoms to the incipient carbene atom at a distance corresponding to the sum of the van der Waals radii of the involved atoms but also depending on the mutual orientation of the interacting groups. A previous estimate for a random approach has set this limit at ca. 4 Å.[21] This benchmark distance was still too long to lead to an unambiguous insertion reaction after carbene formation.[27] Therefore, we reexamined it following the results of analysis of the 100 ps BOMD trajectories of **A1** and **A2** (Figures S7−S9, Supporting Information) in which we counted the encounters of the incipient carbene atom with selected ion atoms over a 2.5−4.5 Å distance. The trajectory contact analysis is shown in Figure 9 and Figure S10 (Supporting Information). Despite their very similar Gibbs energies, the conformers followed different trajectories at both 310 and 640 K (Figure S7−S9). At 310 K, ion **A1** was found to experience 22% contacts with the exchangeable hydrogens within a 3.7 Å distance, which corresponded to the experimental cross-linking yield (21%. Table 1). Interestingly, the number of these contacts decreased upon increasing the ion temperature to 640 K, which can be attributed to a larger conformational space accessed by the ion at higher temperatures, making the specific contacts with exchangeable hydrogens relatively less frequent due to increased contacts with other atoms. The contacts were distributed among the Gly-amide NH (H36), Gly carboxyl OH (H42), and Leu-amide NH (H35). The most acidic proton (H80) showed a lower participation at 310 K which increased at 640 K (green symbols in Figure 9). In contrast, conformer **A2** showed chiefly contacts with the nonexchangeable hydrogen atoms, whereas contacts with the exchangeable protons were very minor at 310 K (Figure S10). Most of the 310 K contacts occurred with the hydrogen atoms of the Ala2 methyl group that accounted for 22% contacts at 3.8 Å. However, while the Ala2 methyl hydrogens were accessible to C18, the methyl carbon atom remained at a > 4.5 Å distance along the entire trajectories, which should hamper insertion into the carbene and formation of the C−C bond. The BOMD trajectory of conformer **A2** was more susceptible to the effective temperature as seen in Figures S7 and S8. At 640 K,

https://doi.org/10.1021/jasms.3c00023
J. Am. Soc. Mass Spectrom. 2023, 34, 763−774

Scheme 4. Proposed Crosslinking Mechanism in s-AAPG Involving the Ala2 Proton

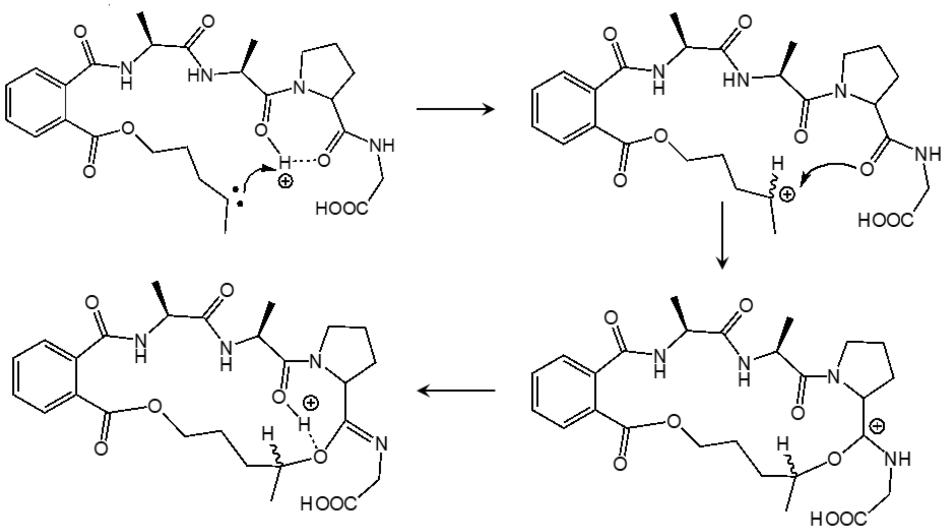

A2 developed numerous contacts with the Gly-amide NH and the charging proton (Figure S10) that could result in proton transfer and cross-linking. Thus, it can be inferred that cross-linking in the nascent, vibrationally hot carbene can involve the Gly amide and Leu OH protons starting from conformer **A2**. Upon collisional cooling, the cross-linking probability in **A2** receded while that of conformer **A1** increased. It should be noted that achieving a close contact was the necessary albeit not a sufficient condition for carbene cross-linking. The accessibility of the other atom of the X−H bond and the energetics of proton transfer were the other factors that likely affected the cross-linking yields and topicity.

Contact analysis of s-AAPG trajectories starting from structures **P1** and **P2** also revealed essential features regarding the conformational dynamics (Figure S11a−f, Supporting Information). A significant fraction of the contacts, when averaged over **P1**−**P3**, involved the Gly-COOH (10%) Gly amide NH (24%), and Pro H_α (15%). However, the Pro-H_α contacts were not associated with contacts with the Pro C_α (e.g., 0% frequency at the 3.5 Å limit) that would be necessary for carbene insertion into the Pro C_α−H_α bond. A large portion of contacts occurred with the OH and NH protons at the protonated Ala2 amide (45% and 2.5%, respectively), which could result in proton transfer to the basic carbene. The high frequency of these contacts was preset by the equilibrium conformations of **P1**−**P3** which were largely fixed by the strong hydrogen bond between the Ala2-OH^+ and the phthalate carbonyl (Figure 8) and which was not disrupted by thermal motion at 350−640 K. Carbene protonation by Ala2-OH^+ can initiate a subsequent nucleophilic attack by the Pro and Gly amide or carboxyl atoms at the transient carbocation, resulting in the macrocyclic ring closure (Scheme 4). The Scheme 4 mechanism was compatible with the results of the cross-linking experiments and the CID-MS^3 spectrum of s-AAPG that showed a marked decrease of peptide chain dissociation at Pro. According to the ion structures shown in Scheme 4, cleavage of the susceptible tertiary peptide bond between Ala2 and Pro in the cross-linked ion cannot lead to the elimination of Pro-Gly which is tethered to the other side chain. Instead, it can trigger elimination of Ala which is the dominant dissociation in the CID-MS^3 spectrum (Figure 4a).

Contact analysis of s-AAHG ion trajectories gave results that were also compatible with the cross-linking data, showing a low efficiency for this peptide sequence. Figure S12a (Supporting Information) shows that conformer **H1** had frequent contacts with the His α-hydrogen that, however, were not accompanied by contacts with the His α-carbon atom. These contacts substantially receded at 640 K (Figure S12b). The other low-energy conformer (**H2**) showed contacts with the Ala1 and Ala2 amide NH at 310 K that were retained at 640 K (Figure S12c,d).

We note that cross-linking to Ala1 and Ala2 amides would not prevent these ions from peptide chain dissociation at the His-Gly sequence that we used in analyzing the CID-MS^3 spectrum in Figure 4b. Thus, the contact analysis may suggest a higher yield of cross-links in s-AAHG than inferred from the interpretation of the CID-MS^3 spectrum. It is noteworthy that in contrast to the solution study,[43] cross-linking to His in gas-phase s-AAHG did not stand out in comparison with the other amino acid residues. This can be ascribed to the fact that the cross-linking yields in gas-phase ions are governed by the ion static and dynamic conformations while not being affected by solvent effects, reagent diffusion, or other condensed-phase factors.

CONCLUSIONS

Peptide scaffolds with covalently attached diazirine carbene precursors were introduced as model molecular systems for studying intramolecular cross-linking to peptide residues. Experimental cross-linking yields showed a dependence on the nature of the amino acid residues. Cross-links to polar groups were found to be prominent, as determined by deuterium incorporation into the carbene site and comparison of CID-MS^n spectra with those of authentic synthetic products. Of the tallied contacts of s-AALG scaffolds, the highest proportion belonged to the Gly residue represented by the carboxyl OH and amide NH. BOMD trajectories were essential in revealing the temperature dependence of the interatomic interactions in thermal ions and provided road maps for tracking close contacts with the incipient carbene atom.

https://doi.org/10.1021/jasms.3c00023
J. Am. Soc. Mass Spectrom. 2023, 34, 763−774

■ ASSOCIATED CONTENT

Supporting Information

The Supporting Information is available free of charge at https://pubs.acs.org/doi/10.1021/jasms.3c00023.

Description of synthetic procedures, NMR spectra, supplementary schemes, and supplementary CID-MS^n spectra (PDF)

■ AUTHOR INFORMATION

Corresponding Author

František Tureček − *Department of Chemistry, Bagley Hall, Box 351700, University of Washington, Seattle, Washington 98195-1700, United States;* orcid.org/0000-0001-7321-7858; Email: turecek@uw.edu

Authors

Hongyi Zhu − *Department of Chemistry, Bagley Hall, Box 351700, University of Washington, Seattle, Washington 98195-1700, United States*

Václav Zima − *Department of Chemistry, Bagley Hall, Box 351700, University of Washington, Seattle, Washington 98195-1700, United States*

Emily R. Ding − *Department of Chemistry, Bagley Hall, Box 351700, University of Washington, Seattle, Washington 98195-1700, United States*

Complete contact information is available at: https://pubs.acs.org/10.1021/jasms.3c00023

Notes

The authors declare no competing financial interest.

■ ACKNOWLEDGMENTS

Research at the University of Washington was supported by the Chemistry Division of the U.S. National Science Foundation, Grant CHE-1951518. F.T. acknowledges support by the Klaus and Mary Ann Saegebarth Endowment.

■ REFERENCES

(1) Liu, M. T. H. *Chemistry of Diazirines*; Vols. *I and II*. CRC Press: Boca Raton, 1987.

(2) Frey, H. M.; Stevens, I. D. R. The Photolysis of Dimethyldiazirine. *J. Chem. Soc.* **1963**, 3514−3519.

(3) Barton, D. H. R.; Jaszberenyi, J. C.; Theodorakis, E. A.; Reibenspies, J. H. The Invention of Radical Reactions. 30. Diazirines as Carbon Radical Traps. Mechanistic Aspects and Synthetic Applications of a Novel and Efficient Amination Process. *J. Am. Chem. Soc.* **1993**, *115*, 8050−8059.

(4) Korneev, S. M. Valence Isomerization between Diazo Compounds and Diazirines. *Eur. J. Org. Chem.* **2011**, *2011*, 6153−6175.

(5) Hashimoto, M.; Hatanaka, Y. Recent Progress in Diazirine-Based Photoaffinity Labeling. *Eur. J. Org. Chem.* **2008**, *2008*, 2513−2523.

(6) Das, J. Aliphatic Diazirines as Photoaffinity Probes for Proteins: Recent Developments. *Chem. Rev.* **2011**, *111*, 4405−4417.

(7) Dubinsky, L.; Bastiaan, P.; Krom, B. P.; Meijler, M. M. Diazirine Based Photoaffinity Labeling. *Bioorg. Med. Chem.* **2012**, *20*, 554−570.

(8) Babu Kumar, A.; Anderson, J. M.; Manetsch, R. Design, Synthesis, and Photoactivation Studies of Fluorous Photolabels. *Org. Biomol. Chem.* **2011**, *9*, 6284−6292.

(9) Rondan, N. G.; Houk, K. N.; Moss, R. A. Transition States and Selectivities of Singlet Carbene Gycloadditions. *J. Am. Chem. Soc.* **1980**, *102*, 1770−1776.

(10) Von E. Doering, W.; Knox, L. H. Comparative Reactivity of Methylene, Carbomethoxycarbene, and Dicarbethoxycarbene toward the Saturated Carbon- Hydrogen Bond. *J. Am. Chem. Soc.* **1961**, *83*, 1989−1992.

(11) Sakai, S. Theoretical Model for the Reaction Mechanisms of Singlet Carbene Analogs into Unsaturated Hydrocarbon and the Origin of the Activation Barrier. *Int. J. Quantum Chem.* **1998**, *70*, 291−302.

(12) Platz, M. S. Atom- Transfer Reactions of Aromatic Carbenes. *Acc. Chem. Res.* **1988**, *21*, 236−242.

(13) Mieusset, J. L.; Brinker, U. H. The Carbene Reactivity Surface: A Classification. *J. Org. Chem.* **2008**, *73*, 1553−1558.

(14) Senthilnathan, V. P.; Platz, M. S. Determination of the Absolute Rates of Decay of Arylcarbenes in Various Low Temperature Matrixes by Electron Spin Resonance Spectroscopy. *J. Am. Chem. Soc.* **1980**, *102*, 7637−7643.

(15) Hadel, L. M.; Maloney, V. M.; Platz, M. S.; McGimpsey, W. G.; Scaiano, J. C. The Absolute Kinetics of Several Reactions of Substituted Diphenylcarbenes. *J. Phys. Chem.* **1986**, *90*, 2488−2491.

(16) Wright, B. B.; Senthilnathan, V. P.; Platz, M. S.; McCurdy, C. W., Jr Tunneling Parameters for the Hydrogen- Atom Abstraction Reactions of Diphenylcarbene in a Low-Temperature Toluene Matrix. *Tetrahedron Lett.* **1982**, *23*, 833−6.

(17) Piersimoni, L.; Kastritis, P. L.; Arlt, C.; Sinz, A. Cross- Linking Mass Spectrometry for Investigating Protein Conformations and Protein- Protein Interactions- A Method for All Seasons. *Chem. Rev.* **2022**, *122*, 7500−7531.

(18) Suchanek, M.; Radzikowska, A.; Thiele, C. Photoleucine and Photomethionine Allow Identification of Protein-Protein Interactions in Living Cells. *Nat. Methods* **2005**, *2*, 261−268.

(19) Iris Biotech, https://www.iris-biotech.de (accessed December 2022).

(20) Yang, T.; Li, X.-M.; Bao, X.; Fung, Y. M. E.; Li, D. Photolysine Captures Proteins that Bind Lysine Post-Translation Modifications. *Nature Chem.Biol.* **2016**, *12*, 70−72.

(21) Shaffer, C. J.; Andrikopoulos, P. C.; Řezáč, J.; Rulíšek, L.; Tureček, F. Efficient Covalent Bond Formation in Gas-Phase Peptide-Peptide Ion Complexes with the Photoleucine Stapler. *J. Am. Soc. Mass Spectrom.* **2016**, *27*, 633−645.

(22) Liu, Y.; Ramey, Z.; Tureček, F. Non-Covalent Interactions of a Neuroprotective Peptide Revealed by Photodissociative Cross-Linking in the Gas Phase. *Chem.—Eur. J.* **2018**, *24*, 9259−9263.

(23) Nguyen, H. T. H.; Andrikopoulos, P. C.; Rulíšek, L.; Shaffer, C. J.; Tureček, F. Photodissociative Cross Linking of Noncovalent Peptide-Peptide Ion Complexes in the Gas Phase. *J. Am. Soc. Mass Spectrom.* **2018**, *29*, 1706−1720.

(24) Nguyen, H. T. H.; Huang, S. R.; Liu, Y.; Liu, Y.; Korn, J. A.; Tureček, F. Probing Arginine-Phosphopeptide Interactions in Non-Covalent Peptide-Peptide Ion Complexes Using Gas-Phase Cross-Linking and Born-Oppenheimer Molecular Dynamics Calculations. *Int. J. Mass Spectrom.* **2019**, *435*, 259−271.

(25) Huang, S. R.; Liu, Y.; Tureček, F. Non-Covalent Complexes of the Amyloid Peptide Fragment Gly-Asn-Asn-Gln-Gln-Asn-Tyr. A Gas-Phase Photodissociative Cross-Linking and Born-Oppenheimer Molecular Dynamics Binding Study. *Phys. Chem. Chem. Phys.* **2019**, *21*, 2046−2056.

(26) Liu, Y.; Tureček, F. Photodissociative Crosslinking of Diazirine-Tagged Peptides with DNA Dinucleotides. *J. Am. Soc. Mass Spectrom.* **2019**, *30*, 1992−2006.

(27) Liu, Y.; Liu, Y.; Nytka, M.; Huang, S. R.; Lemr, K.; Tureček, F. Probing D- and L-Adrenaline Binding to β_2-Adrenoreceptor Peptide Motifs by Photodissociation Crosslinking and Ion Mobility Mass Spectrometry. *J. Am. Soc. Mass Spectrom.* **2021**, *32*, 1041−1052.

(28) Pepin, R.; Shaffer, C. J.; Tureček, F. Position-Tunable Diazirine Tags for Peptide-Peptide Ion Crosslinking in the Gas-Phase. *J. Mass Spectrom.* **2017**, *52*, 557−560.

(29) Jackson, J. E.; Soundararajan, N.; Whie, W.; Liu, M. T. H.; Bonneau, R.; Platz, M. S. Measurement of the Absolute Rate of 1,2-Hydrogen Migration in Benzylchlorocarbene. *J. Am. Chem. Soc.* **1989**, *111*, 6874−6875.

(30) Stevens, I. D. R.; Liu, M. T. H.; Soundararajan, N.; Paike, N. The Barrier for 1,2-Hydrogen Shift in Dialkyl Carbenes. *Tetrahedron Lett.* **1989**, *30*, 481−484.
(31) Sugiyama, M. H.; Celebi, S.; Platz, M. S. A Significant Barrier to 1, 2- Hydrogen Migration in Singlet 1- Phenylethylidene. A Laser Flash Photolysis Study. *J. Am. Chem. Soc.* **1992**, *114*, 966−973.
(32) Celebi, S.; Leyva, S.; Modarelli, D. A.; Platz, M. S. 1, 2-Hydrogen Migration and Alkene Formation in the Photoexcited States of Alkylphenyldiazomethanes. *J. Am. Chem. Soc.* **1993**, *115*, 8613−20.
(33) Pezacki, J. P.; Couture, P.; Dunn, J. A.; Warkentin, J.; Wood, P. D.; Lusztyk, J.; Ford, F.; Platz, M. S. Rate Constants for 1,2-Hydrogen Migration in Cyclohexylidene and in Substituted Cyclohexylidenes. *J. Org. Chem.* **1999**, *64*, 4456−4464.
(34) Marek, A.; Tureček, F. Collision-Induced Dissociation fof Diazirine-Labeled Peptide Ions. Evidence for Brønsted-Acid Assisted Elimination of Nitrogen. *J. Am. Soc. Mass Spectrom.* **2014**, *25*, 778−789.
(35) Kirmse, W. Carbene Protonation. *Adv. Carbene Chem.* **2001**, *3*, 1−151.
(36) Stein, T. H.; Vasiliu, M.; Arduengo, A. J., III; Dixon, D. A. Lewis Acidity and Basicity: Another Measure of Carbene Reactivity. *J. Phys. Chem. A* **2020**, *124*, 6096−6103.
(37) Warner, P. M.; Chu, I. S. Carbene Insertion into Methanol: a Case of Reversible Ylide Formation. *J. Am. Chem. Soc.* **1984**, *106*, 5366−5367.
(38) Dix, E. J.; Goodman, J. L. Protonation of Diarylcarbenes by Alcohols: The Importance of Ion Pair Dynamics. *J. Phys. Chem.* **1994**, *98*, 12609−12612.
(39) Peon, J.; Polshakov, D.; Kohler, B. Solvent Reorganization Controls the Rate of Proton Transfer from Neat Alcohol Solvents to Singlet Diphenylcarbene. *J. Am. Chem. Soc.* **2002**, *124*, 6428−6438.
(40) Abu-Saleh, A. A. A.; Almatarneh, M.; Poirier, R. A. Bimolecular Reactions of Carbenes: Proton Transfer Mechanism. *Chem. Phys. Lett.* **2018**, *698*, 36−40.
(41) Kirmse, W.; Meinert, T.; Modarelli, D. A.; Platz, M. S. Carbenes and the Oxygen- Hydrogen Bond: Bicycloalkylidenes. *J. Am. Chem. Soc.* **1993**, *115*, 8918−27.
(42) Wright, B. B.; Platz, M. S. Chemistry and Kinetics of Aryl Carbenes in Methanol at Low Temperatures. *J. Am. Chem. Soc.* **1984**, *106*, 4175−80.
(43) Ziemianowicz, D. S.; Bomgarden, R.; Etienne, C. W.; Schriemer, D. C. Amino Acid Insertion Frequencies Arising from Photoproducts Generated Using Aliphatic Diazirines. *J. Am. Soc. Mass Spectrom.* **2017**, *28*, 2011−2021.
(44) Iacobucci, C.; Goetze, M.; Piotrowski, C.; Arlt, C.; Rehkamp, A.; Ihling, C.; Hage, C.; Sinz, A. Carboxyl-Photo-Reactive MS Cleavable Cross-Linkers: Unveiling a Hidden Aspect of Diazirine-Based Reagents. *Anal. Chem.* **2018**, *90*, 2805−2809.
(45) Amrich, M. J.; Bell, J. A. Photoisomerization of Diazirine. *J. Am. Chem. Soc.* **1964**, *86*, 292−293.
(46) Voigt, E.; Meier, H. Uber die Valenzisomerie von Diazoverbindungen und Diazirinen. *Chem. Ber.* **1975**, *108*, 3326−3335.
(47) Korneev, S. M. Valence Isomerization between Diazo Compounds and Diazirines. *Eur. J. Org. Chem.* **2011**, *2011*, 6153−6175.
(48) Shaffer, C. J.; Martens, J.; Marek, A.; Oomens, J.; Tureček, F. Photoleucine Survives Backbone Cleavage by Electron Transfer Dissociation. A Near-UV Photodissociation and Infrared Multiphoton Dissociation Action Spectroscopy Study. *J. Am. Soc. Mass Spectrom.* **2016**, *27*, 1176−1185.
(49) Shigdel, U. K.; Zhang, J.; He, C. Diazirine-Based DNA Photo-Cross-Linking Probes for the Study of Protein-DNA Interactions. *Angew. Chem., Int. Ed.* **2008**, *47*, 90−93.
(50) Janz, J. M.; Ren, Y.; Looby, R.; Kazmi, M. A.; Sachdev, P.; Grunbeck, A.; Haggis, L.; Chinnapen, D.; Lin, A. Y.; Seibert, C.; McMurry, T.; Carlson, K. E.; Muir, T. W.; Hunt, S.; Sakmar, T. P. Direct Interaction between an Allosteric Agonist Pepducin and the Chemokine Receptor CXCR4. *J. Am. Chem. Soc.* **2011**, *133*, 15878−15881.
(51) Wan, J.; Brož, B.; Liu, Y.; Huang, S. R.; Marek, A.; Tureček, F. The DNA Radical Code. Resolution of Identity in Dissociations of Trinucleotide Codon Cation Radicals in the Gas Phase. *J. Am. Soc. Mass Spectrom.* **2023**, *34*, 304−319.
(52) Řezáč, J. Cuby: An Integrative Framework for Computational Chemistry. *J. Comput. Chem.* **2016**, *37*, 1230−1237.
(53) Řezáč, J.; Fanfrlík, J.; Salahub, D.; Hobza, P. Semi-Empirical Quantum Chemical PM6Method Augmented by Dispersion and H Bonding Correction Terms Reliably Describes Various Types of Noncovalent Complexes. *J. Chem. Theory Comput.* **2009**, *5*, 1749−1760.
(54) Becke, A. D. Density-Functional Exchange-Energy Approximation with Correct Asymptotic Behavior. *Phys. Rev. A* **1988**, *38*, 3098−3100.
(55) Zhao, Y.; Truhlar, D. G. The M06 Suite of Density Functionals for Main Group Thermochemistry, Thermochemical Kinetics, Noncovalent Interactions, Excited States, and Transition Elements: Two New Functionals and Systematic Testing of Four M06-Class Functionals and 12 Other Functionals. *Theor. Chem. Acc.* **2008**, *120*, 215−241.
(56) Tomasi, J.; Mennucci, B.; Cammi, R. Quantum Mechanical Continuum Solvation Models. *Chem. Rev.* **2005**, *105*, 2999−3093.
(57) Bleiholder, C.; Osbum, S.; Williams, T. D.; Suhai, S.; Van Stipdonk, M.; Harrison, A. G.; Paizs, B. Sequence-Scrambling Fragmentation Pathways of Protonated Peptides. *J. Am. Chem. Soc.* **2008**, *130*, 17774−17789.
(58) Novák, J.; Lemr, K.; Schug, K. A.; Havlíček, V. CycloBranch: De Novo Sequencing of Nonribosomal Peptides from Accurate Product Ion Mass Spectra. *J. Am. Soc. Mass Spectrom.* **2015**, *26*, 1780−1786.
(59) Vaisar, T.; Urban, J. Probing the Proline Effect in CID of Protonated Peptides. *J. Mass Spectrom.* **1996**, *31*, 1185−1187.

https://doi.org/10.1021/jasms.3c00023
J. Am. Soc. Mass Spectrom. 2023, 34, 763−774